Inorganic Chemistry

Article

pubs.acs.org/IC

Crystal Structure and Cyclic Hydrogenation Property of Pr_4MgNi_{19}

Kenji Iwase,*[,†] Naoyoshi Terashita,[‡] Kazuhiro Mori,[§] Hitoshi Yokota,[†] and Tetsuya Suzuki[†]

[†]Department of Materials Science and Engineering, Ibaraki University, 4-12-1, Nakanarusawa, Hitachi, Ibaraki 316-8511, Japan

[‡]Japan Metals & Chemicals Co., Ltd., Nishiokitama-gun, Yamagata 999-1351, Japan

[§]Research Reactor Institute, Kyoto University, 2-1010 Asashiro-nishi, Kumatori, Sennan, Osaka 590-0494, Japan

Supporting Information

ABSTRACT: The hydrogen absorption−desorption property and the crystal structure of Pr_4MgNi_{19} was investigated by pressure−composition isotherm measurement and X-ray diffraction (XRD). Pr_4MgNi_{19} consisted of two phases: 52.9% Ce_5Co_{19}-type structure (3R) and 47.0% Gd_2Co_7-type structure (3R). Sm_5Co_{19}-type structure (2H) and Ce_2Ni_7-type structure (2H) were not observed in the XRD profile. The Mg atoms substituted at the Pr sites in a $MgZn_2$-type cell. The maximum hydrogen capacity reached 1.14 H/M (1.6 mass%) at 2 MPa. The hysteresis factor, Hf = $\ln(P_{abs}/P_{des})$, was 1.50. The cyclic hydrogenation property of Pr_4MgNi_{19} was investigated up to 1000 absorption−desorption cycles. After 250, 500, 750, and 1000 cycles, the retention rates of hydrogen were reduced to 94%, 92%, 91%, and 90%, respectively. These properties were superior to those of Pr_2MgNi_9 and Pr_3MgNi_{14}.

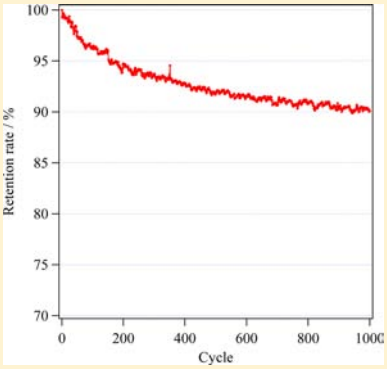

1. INTRODUCTION

La−Mg−Ni alloys have been investigated to improve the hydrogenation property of hydrogen storage materials.[1−3] La−Mg−Ni alloys with superlattice structures indicated that their hydrogen capacity measured by the volumetric method is higher than that of the $LaNi_5$ alloy.[1] Zhang et al. reported the crystal structure and the hydrogenation property of La_4MgNi_{19}.[4] The alloy consists of Sm_5Co_{19}-type and Ce_5Co_{19}-type structures. The maximum hydrogen capacity reached 1.0 H/M (1.5 mass%) at 4 MPa. The wide plateau region was observed between 0.1 and 0.9 H/M. The enthalpy was determined from the van't Hoff plots to be −32.1 kJ/mol H_2 for absorption, which is close to the value for the $LaNi_5$−H_2 system (−30 kJ/mol H_2). The cyclic hydrogenation property of $(La,Mg)_5Ni_{19}$ was reported by Liu et al.[5] The maximum hydrogen capacity after 30 cycles was reduced to 89% of the first cycle, which is inferior to $LaNi_5$.

Crystal structure and pressure−composition (P−C) isotherm of Pr_5Ni_{19} were investigated.[6,7] The present authors reported that the alloy is composed of two phases: Sm_5Co_{19}-type Pr_5Ni_{19} (90 mass%) and $CaCu_5$-type $PrNi_5$ (10 mass%).[6] Sm_5Co_{19}-type Pr_5Ni_{19} consists of cells with the $MgZn_2$- and $CaCu_5$-type structures stacked along the *c* axis in a ratio of 1:3. The maximum hydrogen storage capacity of the first cycle reached 1.1 H/M, but 0.3 H/M of hydrogen remained in the alloy after the first desorption process. Lemort et al. reported the crystal structure and the hydrogenation property of $Pr_{3.75}Mg_{1.25}Ni_{19}$.[8] The alloy consists of three phases of polymorphic Sm_5Co_{19}-type (60%) and Ce_5Co_{19}-type (32%) structures and $PrNi_5$ (8%). It is also found that the Mg atoms substitute for the Pr sites in the $MgZn_2$-type cell in both the Sm_5Co_{19}-type and Ce_5Co_{19}-type structures. The maximum hydrogen capacity reached 1.1 H/M at 10 MPa, and the reaction was reversible during the absorption and desorption processes. The replacement of 25 at% of Pr by Mg leads to a 30% increase of the hydrogen capacity per weight and a decrease of the plateau pressure by half a decade. The cyclic hydrogenation properties of Pr_2MgNi_9 and Pr_3MgNi_{14} have also been reported, which compare favorably with $LaNi_5$.[9,10] The hydrogen occupation in $MgZn_2$- and $CaCu_5$-type cells is related to expansion of those cells volume, which has an effect on hydrogenation property. Pr_3MgNi_{14} indicated the remarkable cyclic property,[10] but the volume expansion of $PrMgNi_4$ and $PrNi_5$ cells were 0.47% and 3.68% after 1000 cycles. $PrMgNi_4$ and $PrNi_5$ cells stacked along the *c* axis in a ratio of 1:2. It is suggested that the $PrMgNi_4$ cell is relaxed $PrNi_5$ cell volume expansion. We expect that the cyclic property improves with increasing the ratio of the $PrNi_5$ cell.

In the present study, we focused on the cyclic property and the structural change of the Pr_4MgNi_{19} alloy. The alloy belongs either to the Sm_5Co_{19}-type structure or the Ce_5Co_{19}-type structure. The structure consists of $PrMgNi_4$ and $PrNi_5$ cells stacked along the *c* axis in a ratio of 1:3. A 2. $PrNi_5$ cell exists between two 1. $PrNi_5$ cells as shown in Figure 1. It is interesting to know the change of volumes of $PrMgNi_4$ and $PrNi_5$ cells and lattice strains during the hydrogen absorption−desorption process.

2. EXPERIMENTAL SECTION

A Pr−Mg−Ni ternary alloy was prepared by induction melting of Pr, Mg, and Ni metals (99.9%) in a high-purity alumina crucible under a

Received: August 29, 2013
Published: December 5, 2013

   dx.doi.org/10.1021/ic402213s | *Inorg. Chem.* 2013, 52, 14270−14274

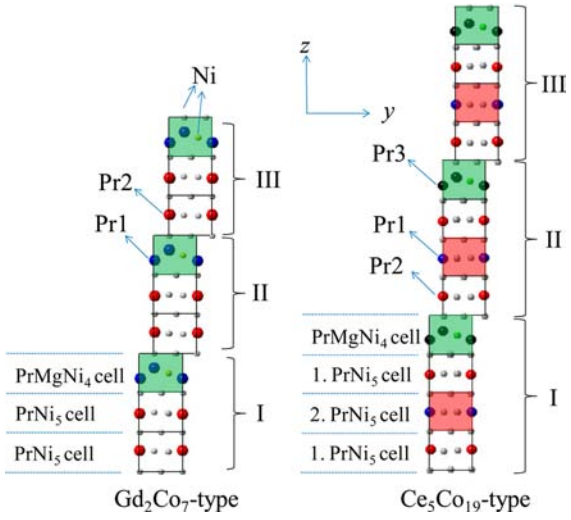

Figure 1. Gd_2Co_7-type (3R) and Ce_5Co_{19}-type (3R) structures.

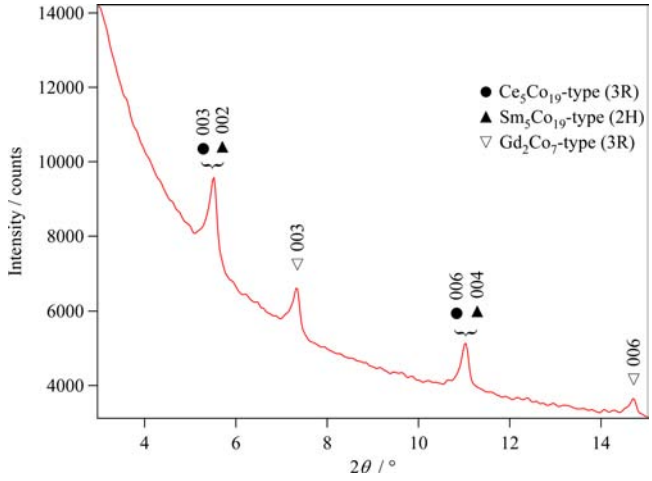

Figure 2. X-ray diffraction (XRD) profile of Pr_4MgNi_{19} in the 2θ region between 3° and 15°.

0.07-MPa helium atmosphere. The obtained Pr−Mg−Ni ingot was annealed at 1343 K for 10 h under an argon atmosphere.

The chemical composition of the starting material was $Pr_4Mg_{1.5}Ni_{19}$. The sample was not sealed under annealing. Mg atoms decreased during heat treatment. The chemical composition of the annealed sample was analyzed using an inductively coupled plasma analyzer. The sample was crashed under air, and then the powder sample was used for ICP. The result indicated a chemical composition of $Pr_{4.03}Mg_{0.96}Ni_{19.05}$.

A powder sample was sieved to a particle size of <20 μm for XRD measurements. The sample was crashed into powder in a mortar under air. The XRD data were collected in step-scan mode using a Rigaku Ultima IV diffractometer. Cu−Kα radiation, monochromatized using a curved graphite crystal, was used. The structural parameters were refined using the Rietveld refinement program RIETAN-2000.[11,12] The reliability of the fitting was judged from the goodness-of-fit parameter S defined as $S = R_{wp}/R_e$, where R_{wp} is the residue of the weighted pattern, and R_e is the statistically expected residue. The peak shape function that was used was a Pseudo−Voigt function containing Gaussian and Lorentzian functions. The anisotropic lattice strain was calculated using the Lorentzian parameter Y_e.[13]

The P−C isotherm was measured by Sieverts' method. The sample for the isotherm measurement was heated in vacuum at 413 K for 1 h and then held at measuring temperatures for 1 h in a stainless-steel container. Hydrogen was introduced at room temperature at 2.0 MPa, and then dehydrogenation was carried out using a rotary pump at 373 K for 1 h. After these processes had been performed three times, the cyclic examination was carried out automatically using a P−C isotherm machine. Fresh hydrogen gas (99.99999% purity) was introduced at each cycle. After each cycle, the sample was dehydrogenated using a rotary pump. The cyclic properties were measured at 313 K up to 1000 cycles.

3. RESULTS

3.1. Rietveld Analysis of Pr_4MgNi_{19}. Figure 2 shows the XRD profile of Pr_4MgNi_{19} in the 2θ region between 3° and 15° in which four superlattice reflections were observed. The d values were 1.6, 1.2, 0.8, and 0.6 nm. The first and third reflections correspond to the Ce_5Co_{19}-type structure (003 and 006) or the Sm_5Co_{19}-type structure (002 and 004). The second and fourth reflections are those of the Gd_2Co_7-type structure (003 and 006). The structure determination of Pr_4MgNi_{19} was carried out by Rietveld refinement of XRD data in the 2θ region between 15° and 85°. At 2θ values around 28°, 30.5°, and 31.5° small peaks from an unknown phase appear, and these data were excluded from the refinement. An initial structural model based on two phases of the Sm_5Co_{19}-type structure (space group $P6_3/mmc$) and the Gd_2Co_7-type structure (space group R-3m) was adopted for the Rietveld refinement. The calculated pattern did not fit well with the observed profile. The goodness-of-fit parameter S was as large as 2.8. The second structural model based on the Ce_5Co_{19}-type structure (space group R-3m) was then adopted, which agreed fairly well with the observed data and S = 2.0. The Ce_5Co_{19}-type structure contains three different Pr sites: Pr1 at the 3a site and Pr2 at the 6c site in the $PrNi_5$ cells and Pr3 at the 6c site in the $PrMgNi_4$ cell. The substituted Mg atoms were located only at the Pr3 sites as shown in Figure 1. The final Rietveld refinement pattern is shown in Figure 3. The mass fractions of the Ce_5Co_{19}- and Gd_2Co_7-type phases were 52.9% and 47.0%, respectively. The structural parameters of the Ce_5Co_{19}-type phase are listed in Table 1.

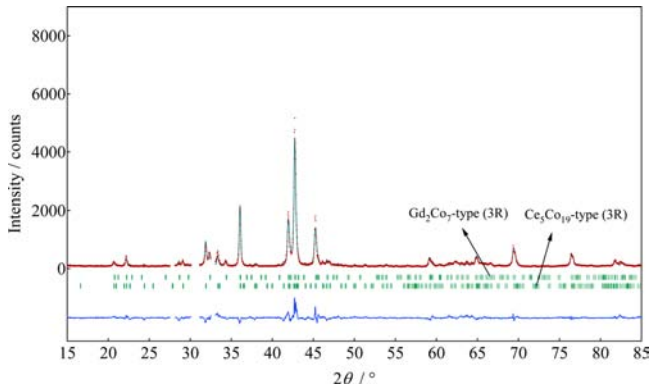

Figure 3. Rietveld refinement pattern of XRD data for Pr_4MgNi_{19}.

3.2. P−C Isotherm of Pr_4MgNi_{19}. The P−C isotherm of Pr_4MgNi_{19} for the first and second absorption−desorption process at 298 K is shown in Figures 4 (a) and (b). In the first cycle, the P−C isotherm was measured with no activation pretreatment. The maximum hydrogen capacity reached 1.14 H/M (1.6 mass%) at 2 MPa in the first absorption. The plateau pressure in the absorption and desorption processes were at P_{abs} = 0.9 MPa and P_{des} = 0.2 MPa. The hysteresis factor defined as Hf = $\ln(P_{abs}/P_{des})$ was 1.50. The plateau region of the first cycle was observed between 0.08 H/M and 0.93 H/M.

dx.doi.org/10.1021/ic402213s | Inorg. Chem. 2013, 52, 14270−14274

Table 1. Structural Parameters of Ce_5Co_{19}-Type Pr_4MgNi_{19} *a*-Space Group: *R*-3*m* (No. 166), $a = 0.4979(1)$ nm, and $c = 4.809(1)$ nm ($R_{wp} = 15.4\%$, $R_I = 7.6\%$, $R_e = 7.7\%$, and $S = 2.0$)

atoms	site	*g*	*x*	*y*	*z*	B ($\times 10^{-2}$ nm^2)
Pr1	3*a*	1	0	0	0	0.9(1)
Pr2	6*c*	1	0	0	0.1577(1)	1.4(3)
Pr3	6*c*	0.500	0	0	0.0810(2)	0.3(6)
Mg	6*c*	0.500	0	0	0.0810(2)	0.3(6)
Ni	3*b*	1	0	0	1/2	0.2(1)
Ni	6*c*	1	0	0	0.2500(0)	0.4(4)
Ni	6*c*	1	0	0	0.3333(0)	0.3(2)
Ni	6*c*	1	0	0	0.4170(4)	0.5(1)
Ni	18*h*	1	0.5000(0)	0.5000(0)	0.1250(2)	0.7(5)
Ni	18*h*	1	0.5000(0)	0.5000(0)	0.0405(2)	0.4(3)

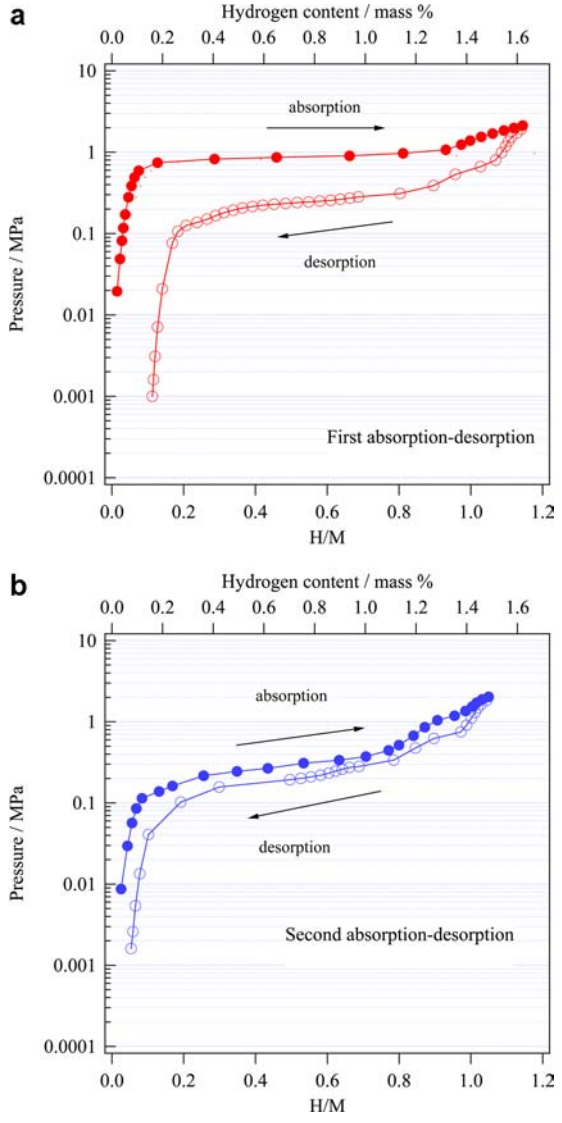

Figure 4. PC isotherm of Pr_4MgNi_{19} at 298 K: (a) first absorption–desorption process and (b) second absorption–desorption process.

The second absorption–desorption process was measured after evacuation at 413 K for 2 h. In the second absorption–desorption process, the absorption pressure decreased from 0.9 to 0.3 MPa.

3.3. Cyclic Absorption–Desorption Property of Pr_4MgNi_{19}. The cyclic property of Pr_4MgNi_{19} up to 1000 cycles is shown in Figure 5. The cyclic test was carried out at

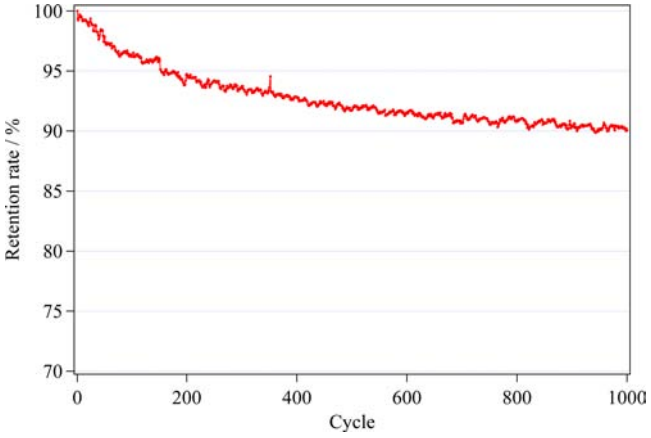

Figure 5. Retention rate of Pr_4MgNi_{19} up to 1000 absorption–desorption processes.

313 K. The retention rate was calculated using the hydrogen capacity of the initial cycle as a reference. After 250, 500, 750, and 1000 cycles, the retention rates were 94%, 92%, 91%, and 90%, respectively. The decrease in the retention rate occurs up to 1000 cycles.

3.4. Crystal Structure after Cyclic Test. After the 1000 absorption–desorption cycles, the sample was examined by XRD. The XRD profile is shown in Figure 6, which is similar to the alloy before hydrogenation. The Bragg peaks broadened slightly in comparison with the original alloy. The two-phase model, which included the Ce_5Co_{19}-type and Gd_2Co_7-type structures, was adopted, and the Rietveld refinement pattern is shown in Figure 6. The pattern was fitted using profile

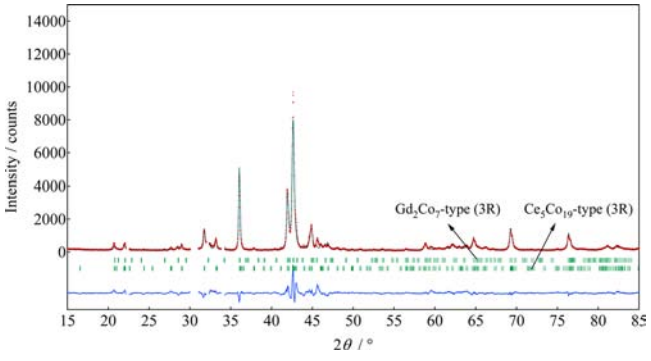

Figure 6. Rietveld refinement of XRD data after 1000 absorption–desorption cycles. The sample contains two phases of Ce_5Co_{19}-type and Gd_2Co_7-type structures.

dx.doi.org/10.1021/ic402213s | Inorg. Chem. 2013, 52, 14270–14274

parameters including the anisotropic broadening parameters X_e (crystallite size) and Y_e (lattice strain) and the isotropic parameter.[13,14] The crystallite size of the alloy before hydrogenation was 300 nm. After the 1000 absorption−desorption cycles, the size decreased to 200 nm. The refined lattice parameters of Pr_4MgNi_{19} with the Ce_5Co_{19}-type structure are a = 0.4985(2) nm, c = 4.852(1) nm; the unit cell volume is V = 1.0443(9) nm^3. The calculated pattern fit well with the observation and S = 3.0.

4. DISCUSSION

4.1. Crystal Structure of Pr_4MgNi_{19}. The present authors investigated the Pr_5Ni_{19} alloy.[6] The crystal structure was studied by XRD and scanning transmission electron microscopy (STEM). Pr_5Ni_{19} exhibits the Sm_5Co_{19}-type (2H). In the present study, however, the structural model used for Pr_4MgNi_{19} was Ce_5Co_{19}-type (3R) with Mg atoms locating only at the Pr3 site of the $MgZn_2$-type cell. The structural model based on two phases of the Ce_5Co_{19}-type and Gd_2Co_7-type structures was adopted for the Rietveld refinement, and a satisfactory fit was obtained. Mass fractions of the Ce_5Co_{19}-type and Gd_2Co_7-type phases were 52.9% and 47.0%, respectively. It is safely concluded that Mg substitution for Pr leads to relative stability of the Ce_5Co_{19}-type (3R) structure. The atomic displacement parameters were shown in Table 1. The value of Pr2 at the 6c site was over 1.0. Pr2 located in the 1. $PrNi_5$ cell. The $PrMgNi_4$ cell is deformed by Mg subsitution, which exsists between the 1. $PrNi_5$ cells. The atomic radius of Pr is larger than that of Mg. The anisotropically strain was formed in the $PrMgNi_4$ cell. It is suggested that the atomic displacement parameters of Pr2 are effected by the anisotropic strain of the $PrMgNi_4$ cell.

Lemort et al. reported the crystal structure of $Pr_{3.75}Mg_{1.25}Ni_{19}$.[8] The sample was prepared by induction melting, and heat treatment was carried out 1173 K for 20 days under argon. $Pr_{3.75}Mg_{1.25}Ni_{19}$ exists in three phases: Sm_5Co_{19}-type (2H), Ce_5Co_{19}-type (3R), and $CaCu_5$-type; the mass fractions of three phases are 60%, 32%, and 8%, respectively. This result does not agree with the present result for Pr_4MgNi_{19} in which the Ce_5Co_{19}-type and Gd_2Co_7-type structures coexist. The reason for the discrepancy can be plausibly attributed to the difference of Mg content of the alloy and the treatment temperature (1343 K for Pr_4MgNi_{19} in the present work).

Zhang et al. investigated the crystal structure of La_4MgNi_{19}.[4] The La_4MgNi_{19} ingot was prepared by induction melting. The obtained ingot was annealed at 1173 K for 48 h and then quenched to room temperature. Sm_5Co_{19}-type (2H) and Ce_5Co_{19}-type (3R) structures coexisted in the XRD profile. The mass fraction of 2H and 3R structures were 43% and 57%, respectively. The result also differs from the binary La_5Ni_{19} compound which exists only in a single 2H phase.[15] As in the case of the La−Mg−Ni ternary system, partial substitution of Mg for La in La_5Ni_{19} favors the formation of the 3R phase.

4.2. Hydrogen Absorption−Desorption Properties. The P−C isotherm of Pr_3MgNi_{14} ternary alloy with a superlattice structure was reported by the present authors.[10] Gd_2Co_7-type (3R) and $PuNi_3$-type (3R) phases coexisted in the alloy with mass fractions of 80% and 20%, respectively. The maximum hydrogen capacity reached 1.12 H/M (1.61 mass%) at 2 MPa. The plateau pressure was 0.1 MPa, and Hf was 1.47. A wide plateau region was observed between 0.14 and 1.00 H/M. The present hydrogenation properties of Pr_4MgNi_{19} such as maximum hydrogen capacity, Hf, and plateau pressure are similar to those of Pr_3MgNi_{14}.

We investigated the hydrogen absorption−desorption property up to 1000 cycles of Pr_2MgNi_9,[9] Pr_3MgNi_{14},[10] and Pr_4MgNi_{19}. The retention rates of these alloys are shown in Table 2. Pr_4MgNi_{19} indicated a retention rate of 90.0% at 1000 cycles, which is superior to those of Pr_2MgNi_9 (85.3%) and Pr_3MgNi_{14} (87.5%). Pr_2MgNi_9 exists in the pure $PuNi_3$-type phase.[9] Pr_3MgNi_{14} contains both Gd_2Co_7-type (80%) and $PuNi_3$-type (20%) phases.[10] In the present Pr_4MgNi_{19} alloy, Ce_5Co_{19}-type (52.9%) and Gd_2Co_7-type (47.0%) phases coexist. From this fact, it is considered that the cyclic property of the Ce_5Co_{19}-type structure is superior to other structures of $PuNi_3$-type and Gd_2Co_7-type.

Table 2. Retention Rate of Pr_2MgNi_9,[9] Pr_3MgNi_{14},[10] and Pr_4MgNi_{19} at 100, 500, and 1000 Cycles

sample	100 cycles	500 cycles	1000 cycles
Pr_2MgNi_9	96.3%	89.4%	85.3%
Pr_3MgNi_{14}	95.3%	89.6%	87.5%
Pr_4MgNi_{19}	96.3%	91.7%	90.0%

4.3. Expansion of $PrMgNi_4$-Type, $PrNi_5$-Type, and Unit Cells after the Cyclic Test. Expansions of lattice parameters and volumes of a unit cell, a $PrMgNi_4$ cell, and a $PrNi_5$ cell of the Ce_5Co_{19}-type structure after 1000 absorption−desorption processes are shown in Table 3.

Table 3. Expansions of Lattice Parameters and Volumes of a Unit Cell, a $PrMgNi_4$ Cell, and a $PrNi_5$ Cell after 1000 Absorption−Desorption Cycles

parameter	value
Pr_4MgNi_{14}	
Ce_5Co_{19}-type	
a	0.12%
c	0.89%
V	1.14%
V ($PrMgNi_4$ cell)	−2.02%
V (1. $PrNi_5$ cell)	4.18%
V (2. $PrNi_5$ cell)	−2.60%

The metal lattice expanded anisotropically, and the expansion is marked along the c axis. The volumes of 1. $PrNi_5$ cells increased in comparison with the original alloy, while $PrMgNi_4$ cells and the 2. $PrNi_5$ cell indicated shrinkage of 2%. It should also be noted that the shrinkage of $PrMgNi_4$ cells and $PrNi_5$ cells after 1000 cycles was not observed in Pr_2MgNi_9[9] and Pr_3MgNi_{14}.[10]

4.4. Anisotropic and Isotropic Lattice Strain. The lattice strain was determined by the Rietveld analysis software RIETAN 2000.[11] The refined isotropic strain parameter (U) and the anisotropic strain parameter (Y_e) were used as the measures of isotropic and anisotropic strains. Nakamura and Akiba reported the lattice strain of $LaNi_{4.75}Al_{0.25}$ during the first hydrogen absorption−desorption process by *in situ* XRD.[16] The full hydride phase showed no anisotropic lattice strain. The isotropic lattice strain was smaller (0.2%) in the hydride alloy than the value (0.4%) for the original alloy. However, anisotropic lattice strain appeared in the hydride phase in the two-phase region of the desorption process. The strain reached 0.6% in the ⟨001⟩ direction.

dx.doi.org/10.1021/ic402213s | *Inorg. Chem.* 2013, 52, 14270−14274

In this study, the retention rate of Pr_4MgNi_{19} reached 90% at 1000 cycles. After 1000 absorption−desorption cycles, the anisotropic broadening vector was determined to be ⟨001⟩, and the anisotropic and isotropic lattice strains were 0.2% and 0.1%, respectively, which do not differ from those after the first activation process. Specifically, the anisotropic and isotropic lattice strains form quickly and are saturated in the first activation process. The refined anisotropic lattice strain is smaller than that of $LaNi_{4.75}Al_{0.25}$.

4.5. Hydrogen Occupation. Nakamura et al. reported the crystal structure of La_4MgNi_{19} deuterided by *in situ* X-ray and neutron powder diffraction.[17] The alloy consisted of 5 phases: 51% Ce_5Co_{19}-type, 19% Pr_5Co_{19}-type, 16% Gd_2Co_7-type, 10% Ce_2Ni_7-type, and 4% $CaCu_5$-type structures. The deuteride phases of the 5:19 and 2:7 compounds kept the symmetry of the original alloy upon deuteration. Unit cells, A_2B_4 cells, AB_5-1 cells, and AB_5-2 cells of the Ce_5Co_{19}-type deuteride expanded almost isotropically. The deuterium content of A_2B_4 cells, AB_5-1 cells, and AB_5-2 cells are 0.98 D/M, 0.82 D/M, and 1.04 D/M, respectively. The change of structural parameters and the volume of a unit cell, the $PrMgNi_4$ cell, the 1. $PrNi_5$ cell, and the 2. $PrNi_5$ cell of Pr_4MgNi_{19} with Ce_5Co_{19}-type as shown in Table 3 after hydrogenation are significantly different from La_4MgNi_{19}. It is particularly interesting to elucidate how hydrogen occupies each $MgZn_2$- and $CaCu_5$-type cell during hydrogenation and how the hydrogen occupation of the cell is related to the hydrogenation properties. The cell expansion corresponds to the amount of hydrogen inserted into each of the cells. Considering the expansion of each cell, the hydrogen occupation of the 1. $PrNi_5$ cell is larger than that of the $PrMgNi_4$ and 2. $PrNi_5$ cells. In particular, the hydrogen occupation and atomic position in the 2. $PrNi_5$ cell is interesting. It is expected that the special hydrogen atomic position and the behavior of cells during hydrogenation is related to the cyclic property. In order to clarify the detailed structural change during hydrogenation, in situ neutron diffraction of Pr−Mg−Ni alloys is under way.

5. CONCLUSIONS

We studied the cyclic property and the structural parameters of Pr_4MgNi_{19}. The retention rate of Pr_4MgNi_{19} after 1000 absorption−desorption processes was greater than those of Pr_2MgNi_9 and Pr_3MgNi_{14}. The refined structural parameters of the original alloy and the dehyrided alloy after the cyclic test was obtained by Rietveld refinement. A satisfactory fit was obtained by using a two-phase model containing Ce_5Co_{19}-type and Gd_2Co_7-type structures for Pr_4MgNi_{19}. The metal lattice of the dehydrided alloy expanded anisotropically along the *c* axis. The volumes of 1. $PrNi_5$ cells increased in comparison with the original alloy, while $PrMgNi_4$ cells and 2. $PrNi_5$ cells indicated shrinkage. The anisotropic lattice strain of the Ce_5Co_{19}-type structure is similar to that of $LaNi_{4.75}Al_{0.25}$. It is known that $LaNi_{4.75}Al_{0.25}$ shows an excellent cyclic property among hydrogen absorbing alloys. The lattice strain of Pr_4MgNi_{19} assures the good cyclic property of hydrogen absorption.

■ ASSOCIATED CONTENT

Ⓢ Supporting Information

cif files. This material is available free of charge via the Internet at http://pubs.acs.org.

■ AUTHOR INFORMATION

Corresponding Author

*Phone: +81-29-287-7189. Fax: +81-29-287-7189. E-mail: fbiwase@mx.ibaraki.ac.jp.

Notes

The authors declare no competing financial interest.

■ ACKNOWLEDGMENTS

The authors thank Emeritus Professor H. Asano (University of Tsukuba) for helpful advice.

■ REFERENCES

(1) Kohno, T.; Yoshida, H.; Kawashima, F.; Inaba, T.; Sakai, I.; Yamanoto, M.; Kanda, M. *J. Alloys Compd.* **2000**, *311*, L5−L7.
(2) Akiba, E.; Hayakawa, H.; Kohno, T. *J. Alloys Compd.* **2006**, *408*−*412*, 280−283.
(3) Yasuoka, S.; Magari, Y.; Murata, T.; Tanaka, T.; Ishida, J.; Nakamura, H.; Nohma, T.; Kihara, M.; Baba, Y.; Teraoka, H. *J. Power Sources* **2006**, *156*, 662−666.
(4) Zhang, Q.; Fang, M.; Si, T.; Fang, F.; Sun, D.; Ouyang, L.; Zhu, M. *J. Phys. Chem. C* **2010**, *114*, 11686−11692.
(5) Liu, Z. Y.; Yan, X. L.; Wang, N.; Chai, Y. J.; Hou, D. L. *Int. J. Hydrogen Energy* **2011**, *36*, 4370−4374.
(6) Iwase, K.; Sakaki, K.; Matsuda, J.; Nakamura, Y.; Ishigaki, T.; Akiba, E. *Inorg. Chem.* **2011**, *50*, 4548−4552.
(7) Lemort, L.; Latroche, M.; Knosp, B.; Bernard, P. *J. Alloys Compd.* **2011**, *509S*, S823−S826.
(8) Lemort, L.; Latroche, M.; Knosp, B.; Bernard, P. *J. Phys. Chem. C* **2011**, *115*, 19437−19444.
(9) Iwase, K.; Terashita, N.; Mori, K.; Tsunokake, S.; Ishigaki, T. *Int. J. Hydrogen Energy* **2012**, *37*, 18095−18100.
(10) Iwase, K.; Terashita, N.; Mori, K.; Ishigaki, T. *Inorg. Chem.* **2012**, *51*, 11805−11810.
(11) Izumi, F. *Rigaku J.* **2000**, *17*, 34−45.
(12) Izumi, F. In *The Rietveld Method*; Young, R. A., Ed.; International Union of Crystallography, Oxford University Press: New York, 1993; pp 236−253.
(13) Willianson, G. K. *Acta Metall.* **1953**, *1*, 22−31.
(14) Patterson, A. L. *Phys. Rev.* **1939**, *56*, 978−982.
(15) Ferey, A.; Cuevas, F.; Latroche, M.; Knosp, B.; Bernard, P. *Electrochim. Acta* **2009**, *54*, 1710−1714.
(16) Nakamura, Y.; Akiba, E. *J. Alloys Compd.* **2000**, *308*, 309−318.
(17) Nakamura, J.; Iwase, K.; Hayakawa, H.; Nakamura, Y.; Akiba, E. *J. Phys. Chem. C* **2009**, *113*, 5853−5859.